Magnetic effect for electrochemically driven cellular convection

Seiichiro Nakabayashi,* Kiyoshi Inokuma, and Antonis Karantonis

Department of Chemistry, Faculty of Science, Saitama University, Urawa, Saitama 338-8570, Japan

(Received 21 December 1998)

Hydrodynamic instability analogous to Rayleigh-Bénard convection is observed in an electrolytic solution between two parallel copper wire electrodes. The laser interferometric technique can reveal the dissipation structure created by the motion of the fluid, which is controlled electrochemically. It is shown that under the presence of horizontal magnetic field the roll cells move horizontally along the electrodes. The electrochemically driven convection is simply controlled and monitored by setting and measuring the electrochemical parameters and forms many kinds of spatiotemporal patterns, especially under the magnetic field. The phenomenon is modeled by considering a Boussinesq fluid under a concentration gradient. The stability of the resulting equations is studied by linear stability analysis. The time dependent nonlinear system is investigated numerically and the main features of the experimental response are reproduced. [S1063-651X(99)05006-0]

PACS number(s): 05.45.−a, 47.54.+r

I. INTRODUCTION

One of the most exotic functions of nature is spontaneous pattern formation in spatial as well as temporal regions. Chemical processes evolving into pattern generation, such as the homogeneous Belouzov-Zhabotinsky reaction [1] and the heterogeneous CO/O_2 reaction on platinum surface [2,3], are rather common. Physicochemical investigation of these reaction mechanisms is in the process of providing a deeper understanding of biological systems which sustain themselves in dissipating the chemical energies [4–6].

We have focused our interest on nonlinear electrochemical systems where electric energy is converting into chemical energies and vice versa. The surface reaction including an electron transfer is driven by the applied potential on the electrode. The electrochemical interface is open for transportation of the reacting species and the reaction is controlled and monitored by electronic circuits. There have been a lot of interesting examples reporting dissipation structures in electrochemical systems [7–9].

The most historical and famous dissipation structure must be Rayleigh-Bénard convection, which is driven by the hydrodynamic instability made by spatial distribution of the temperature. It has been observed experimentally, analytically, and numerically, that when the parameters of this system reach a critical value, fluid convection starts, which may form a variety of spatial patterns [10,11]. By varying the bifurcation parameters even further, new types of bifurcations and resonance lead to spatiotemporal periodicities, symmetry breaking, or even chaos. Related work on other hydrodynamic systems, such as driven flows [12–21], magnetoconvection [22–24], and forced thermal convection [25], revealed similar and even richer dynamical behavior when an external force, other than gravity, is applied to the system. The large amount of research in the field of hydrodynamic instabilities has illuminated, to some extent, the physical processes behind certain instabilities leading to pattern formation, new routes to the transition from one kind of behavior

to another, and possible reduced mathematical models which are able to reproduce to some extent the physical response of these systems [26].

In this article, we will present an analog of Rayleigh-Bénard convection, which is controlled electrochemically. The system consists of an electrolytic solution lying between two wire copper electrodes. The main difference between the Rayleigh-Bénard system and the present one is that in the electrochemical cell heterogeneous chemical reactions occur on the electrodes' surfaces. Hence, under certain conditions discussed in this work, the role of the temperature gradient is now played by a concentration gradient between the two electrodes. The temperature difference between the two wire electrodes can be assumed constant and thus the density variation in the gravitational field is now due to the concentration in the electrolytic solution and not due to the temperature.

An additional external forcing is also considered in the present work, namely, the Lorenz body force due to a constant horizontal magnetic field. It is shown that this additional forcing induces new types of response, very similar to other hydrodynamic systems where no chemical reactions are occurring. The actual effect of the constant magnetic field is investigated experimentally and theoretically and the new types of fluid motion are discussed.

The paper is organized as follows. In Sec. II the experimental arrangement is presented. The experimental results, both in the absence and the presence of the magnetic field, are described in Sec. III. In Sec. IV the model equations are presented and studied both analytically and numerically. Finally, in Sec. V the results are discussed.

II. EXPERIMENTAL ARRANGEMENT

The configuration of the electrochemical cell is shown at the lower right of Fig. 1. The two electrodes were copper wires, whose diameter was about 0.5 mm. The electrodes were placed parallel between two quartz windows. The distance between the electrodes was about 0.3 mm. The quartz windows were connected to each other with two O-rings.
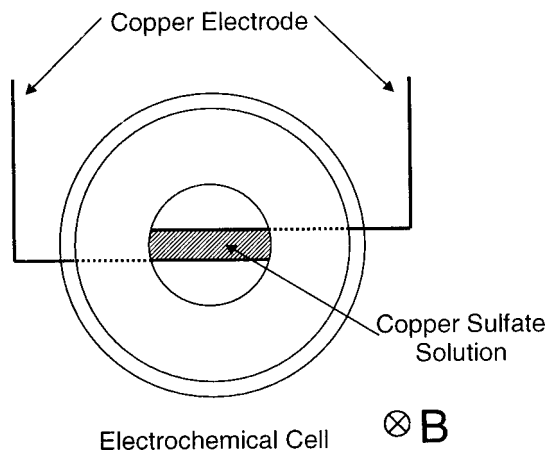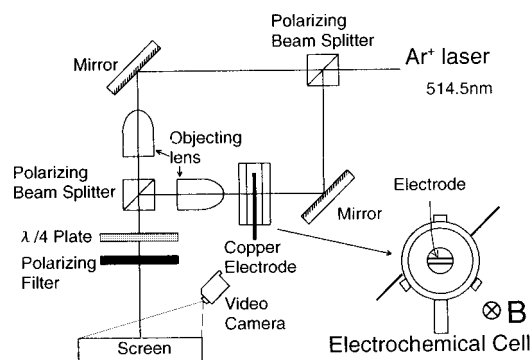
---

*Author to whom correspondence should be addressed.

FIG. 1. Optical arrangement of Mach-Zehnder laser interferometer and the electrochemical cell.
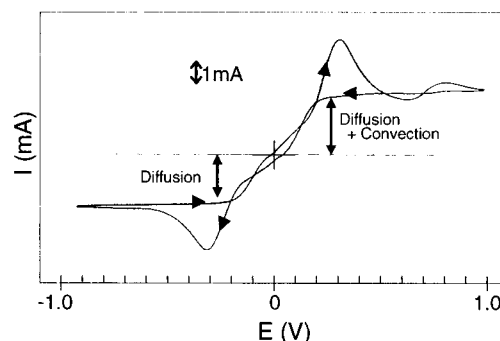

FIG. 2. Relationship between the current and the potential. The potential is represented as the upper electrode potential with respect to that of the lower electrode. Sweep rate: 50 mV/s.

III. EXPERIMENTAL RESULTS

A. Under no magnetic field

Thus, a closed cell was formed where the distance between the quartz windows was 2 mm. The diameter of the windows as well as the length of the electrodes was 20 mm. The direction along the electrodes was the x direction. The plane defined by the two electrodes was placed parallel to the direction of the gravity field, which was considered the z direction. The electrolyte solution used was an aqueous solution containing $0.1M$ $CuSO_4$ and $0.2M$ Na_2SO_4. The electrochemical parameters were controlled by a potentiostat. The current and potential were recorded on an X-Y recorder. A magnetic field was generated by a Helmholtz coil, connected to a power supply. The strength of a magnetic field was measured by a Gauss meter. The direction of the magnetic field was normal to the plane defined by the two electrodes.

A Mach-Zehnder laser interferometer was used to observe the motion of the electrolyte [27,28]. The optical arrangement is shown in Fig. 1. The coherent emission of 514.5 nm from an Ar^+ laser was divided into two beams by a polarizing beam splitter. One of them, reflected by a mirror, passed through the electrolyte solution between the two electrodes. The other beam was reflected by a mirror, and the two beams were again combined at a final polarizing beam splitter. After that, the interferogram was projected on the screen and recorded by a video camera. This setup achieved a vertical cross sectional view of the spatial distribution of the refractive index in the electrolyte solution. Because the refractive index of the solution is proportional to the concentration of Cu^{2+} up to $1.2M$, the fringes in the interferogram are considered as the contour lines of the concentration.

A typical relationship between the current and the potential applied between the two parallel copper electrodes is shown in Fig. 2. The horizontal axis represents the potential difference between the upper electrode potential, E_1, and the lower electrode potential, E_2; i.e., $E = E_1 - E_2$. In the positive potential region, electrodissolution proceeds at the upper electrode and electrodeposition at the lower electrode. In the negative potential region, the reverse reaction takes place, i.e., electrodissolution at the lower electrode and electrodeposition at the upper electrode. The potential sweep rate was 50 mV/s. The potential is scanned repeatedly between $+1.0$ and -1.0 V. After the current response becomes stable, the cyclic voltammogram is recorded. On the way of the potential scanning to the positive direction, a small oscillation is observed and a current becomes steady (3.0 mA) after a current maximum at $+0.31$ V. On the negative potential scanning, the current becomes steady (2.3 mA) following a current maximum at -0.32 V. There is no oscillation in this region. When the potential is reversing, i.e., on the negative potential scanning in the positive potential region, the saturation currents are obtained. These saturated currents are governed by the mass transport of copper ions. The value of the saturated current in the positive potential region is larger than the one in the negative potential region because the copper ion is transported by diffusion and convection in the positive potential region, whereas it is transported only by diffusion in the negative potential region.

Typical interferograms under no magnetic field are shown in Fig. 3. The potential is $+0.4$ V for Fig. 3(a) and -0.4 V for Fig. 3(b). In Fig. 3(a), the electrodissolution proceeds at the upper electrode. In this case convection is observed, with upward and downward streams ranged regularly in space. In Fig. 3(b) the electrodissolution proceeds at the lower electrode. The horizontal fringes are ranged along the electrode. In this case there is no convection, and the ions are transported from the lower to the upper electrode by diffusion, which proceeds in the concentration gradient. Convection occurs specifically when the concentration of copper ions makes an unstable distribution of the fluid density under the gravitational field [Fig. 3(a)].
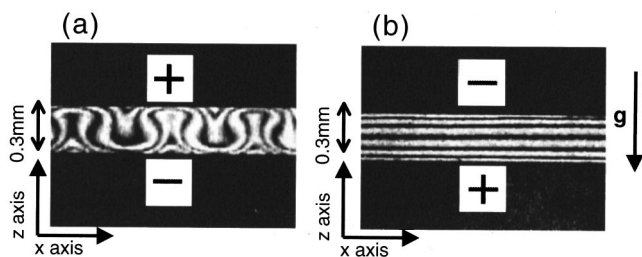
FIG. 3. Vertical cross sectional view of the concentration of the copper sulfate obtained by the laser interferometer. (a) When the anode is on the top ($E = +0.4$ V), fluid convection is observed; and (b) when the anode is at the bottom ($E = -0.4$ V) ions are moving only due to diffusion.

B. Under magnetic field

The time evolution of the interferograms is shown in Fig. 4, where the magnetic field strength is 112 G and the potential is $+0.4$ V. In order to prevent any edge effects, each picture in Fig. 4 is taken in the middle part of the electrolytic cell at time intervals of 3 s. It is found that the roll cells are moving horizontally from left to right and the direction of streams is slightly tilted from the one obtained under only gravitational field. As the ionic current is passing through the electrolyte between the two electrodes, Lorenz force moves the roll cells towards the right. The relationship between the velocity of the roll cells and the magnetic field strength is shown in Fig. 5. The velocity of the roll cells increases proportionally to the magnetic field strength. The roll cells do not break and move smoothly when the magnetic field does not exceed the value of 187 G. However, over 187 G, the magnetic field perfectly destroyed the cells.

The interferograms under several values of the magnetic field strength are shown in Fig. 6. The shape of the interferograms is not changed up to 187 G in Fig. 6(a), where the applied potential is -0.4 V. The fluid between the two electrodes moves towards the right due to the magnetohydrodynamic force. This movement of the fluid does not disturb the spatial distribution of the concentration of the copper ion, which concludes the motion to be a luminar flow. However, when the potential is $+0.4$ V, the shape of the interferograms varies as a function of the magnetic field strength; the
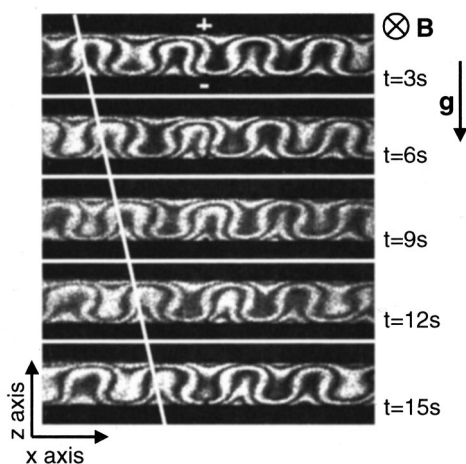

FIG. 4. Time evolution of the interferogram under the magnetic field. $B = 112$ G, $E = +0.4$ V.
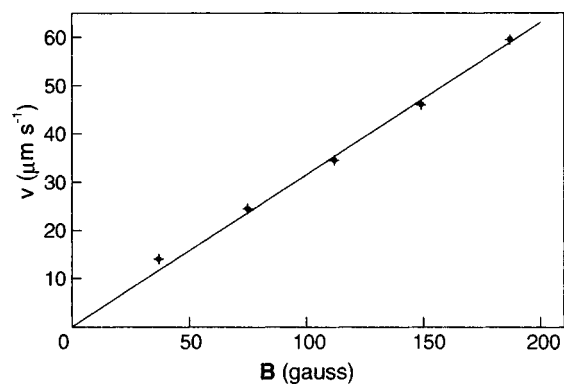

FIG. 5. Relationship between the traveling velocity of the rolls and the strength of the magnetic field. $E = +0.4$ V.

roll cells are stretched towards the lateral direction. The horizontal length of the cell is enlarged and the fluid patterns are tilted as the field strength is increasing. Although the shape of the interferogram varies, especially in the positive potential region, the relationship between the current and potential is identical to the one shown in Fig. 2 under magnetic field strength of 149 G.

Considering that the shape of the interferogram varies as a function of the magnetic field, the transient behavior of the fluid motion was investigated by turning off the magnetic field. The time evolution of the interferogram before and after the disappearance of the magnetic field is shown in Fig. 7, where the magnetic field strength is 149 G and the potential is $+0.4$ V. The pictures in Fig. 7 are taken at time intervals of every 3 s. In order to avoid the inductive effect, the induction current from the magnet was blocked by the diode inserted between the magnet and the output terminal of the power supply. Under the magnetic field, the roll cells are moving from left to right. After the magnetic field disappeared, the cells start to move in the reverse direction, as shown by the line in Fig. 7. Because the stretching force disappears after the termination of the magnetic field, the roll cells are compressed up to the zero field shape, which must be the origin of this reverse motion.

In order to investigate an edge effect, the time evolution of the interferograms was obtained at the edge of the electrodes and shown in Fig. 8, where the magnetic strength is 112 G and the potential is $+0.4$ V. The pictures in Fig. 8 are obtained at time intervals of every 2 s. At both ends of the electrodes, plastic spacers were inserted between the two electrodes. This spacer partly prevents the horizontal movement of the fluid. At the edge, the fluid must pass through the space between the electrodes and the optical windows. At the edge of the electrode, as the conductance of the fluid decreases, the lateral velocity decreases as shown by the line in the right of Fig. 8. Because the roll cells cannot move smoothly at the end of the electrode, they push each other and disappear. As is shown by the two lines in Fig. 8, the streams in the left move more quickly and they catch up to the one in the right. It is found that an up flow between two down streams disappears and these three streams merge into one down flow. This is the way in which roll cells disappear at the end of closed boundaries.

In the case of the open boundaries at the end of the electrodes, the motion was different from the one at the closed
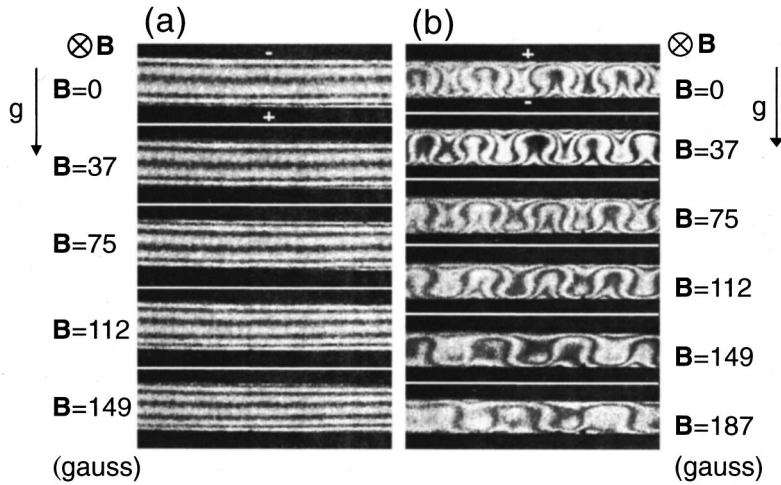
FIG. 6. Comparison of the interferograms under magnetic field. (a) Top electrode is a cathode ($E = -0.4$ V); and (b) top electrode is an anode ($E = +0.4$ V) where traveling, tilting, and stretching of the rolls is observed.

boundaries. In this case, the edges of the two electrodes were painted in order to insulate electronically. Within this coated area at the edge of the electrodes, neither the electrochemical reaction or the convection occurs, but the conductance of the lateral movement of the fluid does not decrease. In this situation, the velocity of the roll cells is constant spatially as shown by the two lines in Fig. 9, where the roll cells disappear without any interaction with others.

IV. THEORETICAL RESULTS

A. Under no magnetic field

During the heterogeneous chemical reactions on the electrode surface, the ionic concentrations change in the neighborhood of the electrodes. The change of concentration leads to the change of the density closer to the electrode surface. The density difference causes a spontaneous movement of the electrolytic solution in the electrochemical cell. This phenomenon is often addressed in electrochemistry as natural convection, independently of the direction of the reaction surface [29].

Let us consider a solution containing a binary electrolyte. The fluxes of the ionic species are

$$\mathbf{j}_1 = -D_1 \mathbf{\nabla} c_1 - \gamma_1 z_1 F c_1 \mathbf{\nabla} \phi + c_1 \mathbf{u}, \tag{1a}$$

$$\mathbf{j}_2 = -D_2 \mathbf{\nabla} c_2 + \gamma_2 z_2 F c_2 \mathbf{\nabla} \phi + c_2 \mathbf{u}, \tag{1b}$$

where the subscripts 1, 2 refer to the cations and anions, respectively, z_i is the absolute value of the charge of the ions, γ_i the ionic mobility, D_i the diffusion coefficient, $c_i(\mathbf{x};t)$ the concentration, $\phi(\mathbf{x};t)$ the electric potential, $\mathbf{u}(\mathbf{x};t)$ the velocity of the solution, and F the Faraday constant.

The solution is electrically neutral, hence,

$$z_1 c_1 - z_2 c_2 = 0. \tag{1c}$$

By using the electroneutrality condition, Eq. (1c), the mass balance equation for the ionic species is written

$$\frac{\partial c}{\partial t} + \mathbf{u} \cdot \mathbf{\nabla} c = D \nabla^2 c, \tag{2}$$

where c is given by

$$c = c_1/z_2 = c_2/z_1, \tag{3}$$

and D is the effective diffusion coefficient,

$$D = \frac{D_1 D_2 (z_1 + z_2)}{D_1 z_1 + D_2 z_2}. \tag{4}$$

It is interesting to note that in the case of a binary electrolyte, a potential term does not enter the mass balance equation. However, this equation does not contain a true diffusion coefficient but an effective one. The potential effect may be considered through the boundary conditions, if the reaction on the electrode is slower than the ionic transport in the solution.
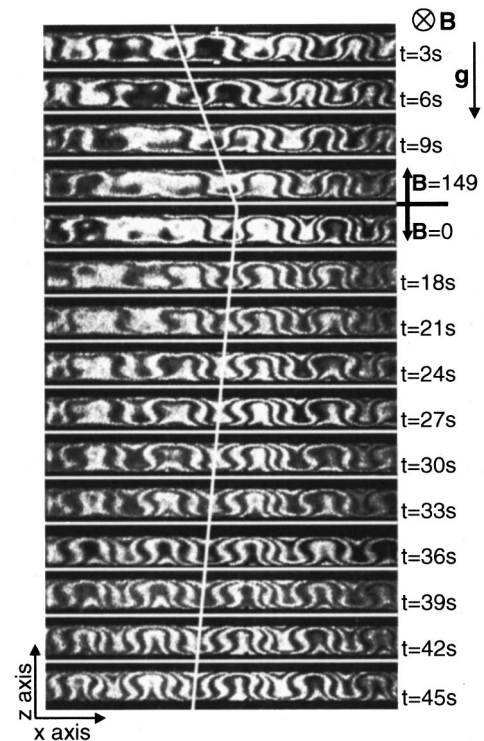

FIG. 7. Transient behavior of the interferogram induced by switching off the magnetic field. $B = 149$ G and $E = +0.4$ V.
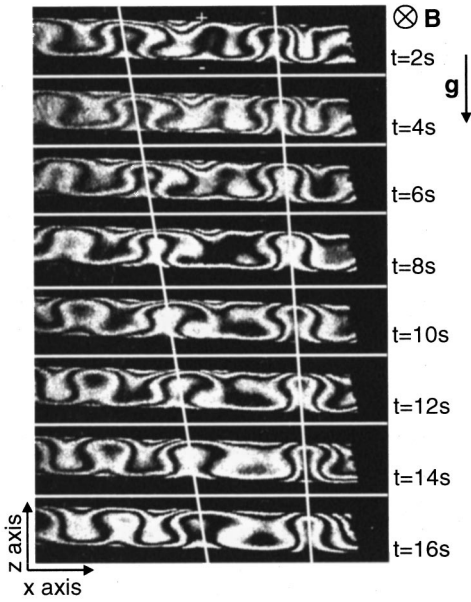
FIG. 8. Movement of the roll cells at a closed edge. $B = 112$ G and $E = +0.4$ V.

FIG. 9. Movement of the roll cells at an open edge. $B = 112$ G and $E = +0.4$ V.

The velocity of the solution, $\mathbf{u}$, is given by the Navier-Stokes equations. Additional, we assume incompressibility, thus,

$$\nabla \cdot \mathbf{u} = 0, \qquad (5a)$$

$$\frac{\partial \mathbf{u}}{\partial t} + \mathbf{u} \cdot \nabla \mathbf{u} = -\frac{1}{\rho_0} \nabla p + v \nabla^2 \mathbf{u} + \frac{\rho}{\rho_0} \mathbf{G}(\mathbf{x}, t), \qquad (5b)$$

where $\rho(c)$ is the density of the solution, p is the (scalar) pressure defined by the equation of state, v is the kinematic viscosity, and $\mathbf{G}(\mathbf{x}, t)$ is the external forces acting on the solution. In Eq. (5b), we use the Boussinesq approximation, that is, $\rho = \rho_0$, in every term of the equation except the force term.

Furthermore, we assume that the density of the solution is given by a truncated Taylor series [29],

$$\rho(c) = \rho_0[1 + \alpha(c - c_0)], \qquad (6)$$

where $\alpha = (1/\rho_0)(\partial \rho / \partial c)|_{c = c_0} > 0$ can be considered as a concentration coefficient of volume expansion and ρ_0 is the solution density when $c = c_0$.

Finally, we introduce a further assumption for the reaction surfaces,

$$c = c_{\text{sat}} \quad \text{(on the anode)}, \qquad (7a)$$

$$c = 0 \quad \text{(on the cathode)}. \qquad (7b)$$

Equations (7) have the following meaning: for both electrode surfaces we consider that the electron transfer step is much faster than the movement of the ions towards or from the surfaces. Thus, on the anode where electrodissolution occurs, ions are concentrated until a saturation value is achieved. On the cathode, all ionic species arriving at the electrode surface are consumed by reduction and thus, the concentration on this surface is zero [29].
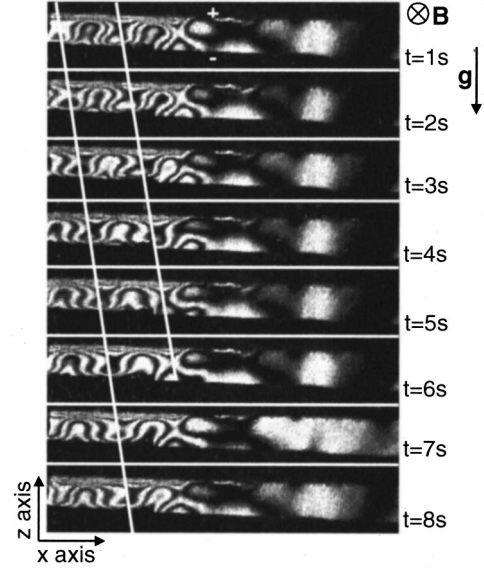
In order to investigate the possible occurrence of hydrodynamic instability, we consider an initial state of the solution where the concentration is uniform and constant along the electrode surfaces. We also do not consider any magnetic field effects, at the first stage. Thus, the basic state whose stability is to be tested is a motionless steady state with a linear concentration gradient along the vertical axis (z axis). The resulting equations for the perturbations of the velocity and the concentration, in dimensionless form and by keeping the same symbols, are

$$\nabla \cdot \mathbf{u} = 0, \qquad (8a)$$

$$\frac{\partial \mathbf{u}}{\partial t} + \mathbf{u} \cdot \nabla \mathbf{u} = -\nabla p + \nabla^2 \mathbf{u} - \frac{R_{\text{el}}}{P_{\text{el}}} c \mathbf{e}, \qquad (8b)$$

$$\frac{\partial c}{\partial t} + \mathbf{u} \cdot \nabla c = -\mathbf{u} + P_{\text{el}}^{-1} \nabla^2 c, \qquad (8c)$$

where the usual parametrization is used: $t \rightarrow \delta^2 t / v$, $\mathbf{u} \rightarrow v \mathbf{u} / \delta$, $c \rightarrow \beta \delta c$, and $\mathbf{x} \rightarrow \delta \mathbf{x}$. In Eqs. (8), $P_{\text{el}} = v / D$ is the "electrochemical" Prandtl number (actually the Schmidt number), $R_{\text{el}} = g \alpha \beta \delta^4 / v D$ is the "electrochemical" Rayleigh number, and $\mathbf{e} = (0,0,1)$. In the expression R_{el}, $\beta = c_{\text{sat}} / \delta$ is the constant concentration gradient between the electrodes, g is the gravity, and δ is the distance between the electrodes.

The stability of Eqs. (8) can be studied by following procedures similar to Chandrasekhar [11]. As is expected, the minimum "electrochemical" Rayleigh number ($R_{\text{el}} \approx 1707.76$) is obtained for a wave number close to 3.12, when rigid boundary conditions are considered. Hence, for this critical R_{el} we expect hydrodynamic instability to occur in the electrochemical system.

The linearized system is expected to have roll solutions for the velocity. Actually, in Fig. 10(a) we present the patterns emerging close to critically for the concentration. In this figure, regions of high concentration are depicted with
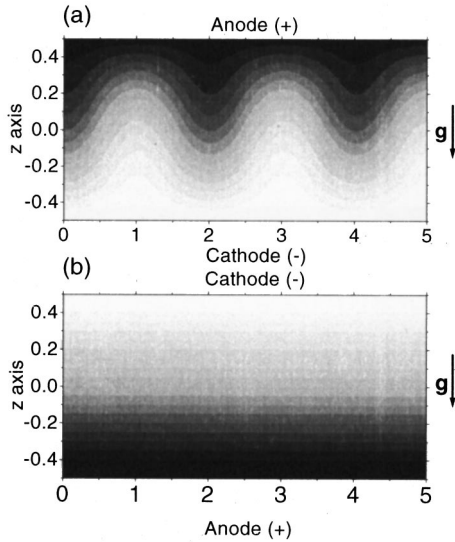
FIG. 10. The concentration profile on criticality: (a) When the anode is on the top, the ions move due to diffusion and convection; and (b) when the anode is at the bottom the ions move only due to diffusion; no fluid convection is observed.

dark gray color whereas regions of low concentration are depicted with light gray color. As can be seen in this figure, while the fluid velocity attains the usual roll solution, the concentration has a stationary wave form profile where the mean amplitude increases from the bottom (cathode) to the top (anode). This profile is the one observed with the interferometric technique. The calculated pattern is in very good qualitative agreement with the experimental evidence presented in Sec. II A [30] and verifies our assumptions for the formulation of the model.

Let us turn now in the case where the upper electrode is a cathode and the lower electrode is an anode. In this case we do not expect a transition from the steady state $\bar{\mathbf{u}} = 0$ to convective flow. The movement of the ions in the solution will only be due to diffusion, that is, Eq. (2) becomes

$$\frac{\partial c}{\partial t} = D\nabla^2 c. \tag{9}$$

The concentration distribution in the case of pure diffusion is presented in Fig. 10(b). As can be seen in this figure, the concentration profile decreases smoothly from the bottom (anode) to the top (cathode). This result is also in very good agreement with the experimental evidence of Sec. III A. A constant concentration gradient was observed between the bottom and the top electrode due to the diffusion of the ionic species from regions of high concentration to regions of low concentration [30].

In order to calculate the time dependence of the concentration profile in the nonlinear case we utilize a numerical procedure. Thus, we assume no y dependence of the variables (i.e., two dimensional case) under Boussinesq approximation. For the numerical scheme we implement the more unrealistic case of both free surface boundary conditions, having in mind that the results differ only quantitatively when the more realistic rigid surface boundary conditions are applied [31]. We also introduce the stream function, $\psi(x,z)$, such as

$$u_x = -\frac{\partial \psi}{\partial z}, \qquad u_z = \frac{\partial \psi}{\partial x}. \tag{10}$$

The dimensionless equations in the two dimensional case are written

$$\frac{\partial}{\partial t}(\nabla^2 \psi) + \frac{\partial(\psi, \nabla^2 \psi)}{\partial(x,z)} = \nabla^4 \psi - \frac{R_{el}}{P_{el}}\frac{\partial c}{\partial x}, \tag{11a}$$

$$\frac{\partial c}{\partial t} - \frac{\partial \psi}{\partial z}\frac{\partial c}{\partial x} + \frac{\partial \psi}{\partial x}\frac{\partial c}{\partial z} = -\frac{\partial \psi}{\partial x} + \frac{1}{P_{el}}\left(\frac{\partial^2 c}{\partial x^2} + \frac{\partial^2 c}{\partial^2 z}\right), \tag{11b}$$

where the symbols have their usual meanings [32]. In order to solve Eqs. (11) numerically, we implement a procedure similar to that of Getling [33]. Therefore, we assume a Fourier expansion in the z direction (normal to the electrodes' surface) and continuous wave number spectra in the x direction (along the electrodes' surface). In this sense, the horizontal dependence of the velocity and the concentration are not assumed periodic. They have continuous spectra and are represented by Fourier integrals. Thus, the stream function and the concentration are written

$$\psi(x,z;t) = \sum_{n=-\infty}^{+\infty} \int_{-\infty}^{+\infty} \tilde{\psi}_n(\omega,t)e^{i(n\pi z + \omega x)}d\omega, \tag{12a}$$

$$c(x,z;t) = \sum_{n=-\infty}^{+\infty} \int_{-\infty}^{+\infty} \tilde{c}_n(\omega,t)e^{i(n\pi z + \omega x)}d\omega. \tag{12b}$$

By taking the Fourier transform of Eqs. (11) and using Eqs. (12) we arrive to the following infinite dimensional system of ordinary differential equations for the spectral functions $\tilde{\psi}_n(\omega,t)$ and $\tilde{c}_n(\omega,t)$:

$$\kappa_n(\omega)\frac{d\tilde{\psi}_n(\omega)}{dt} = -\kappa_n^2(\omega)\tilde{\psi}_n(\omega) + i\omega\frac{R_{el}}{P_{el}}\tilde{c}_n(\omega) + K_n(\omega), \tag{13a}$$

$$\frac{d\tilde{c}_n(\omega)}{dt} = -i\omega\tilde{\psi}_n(\omega) - \frac{\kappa_n(\omega)}{P_{el}}\tilde{c}_n(\omega) + L_n(\omega), \tag{13b}$$

where $\kappa_n(\omega) = \omega^2 + n^2\pi^2$, and

$$K_n(\omega) = \sum_{m=-\infty}^{+\infty} \int_{-\infty}^{+\infty} (\omega m - n\alpha)\pi\kappa_m(\alpha)\tilde{\psi}_{n-m}(\omega - \alpha)\tilde{\psi}_m(\alpha)d\alpha, \tag{14a}$$

$$L_n(\omega) = \sum_{m=-\infty}^{+\infty} \int_{-\infty}^{+\infty} (\omega m - n\alpha)\pi\tilde{\psi}_{n-m}(\omega - \alpha)\tilde{c}_m(\alpha)d\alpha. \tag{14b}$$

Equations (13) are solved by writing separately real and imaginary parts and introducing a finite range of the parameters n and ω. In the present work, a grid of 5×80 points is used and thus a total number of 4×81 equations are integrated for each n value. The temporal integration is performed by a Runge-Kutta fourth order scheme whereas the integrals $K_n(\omega), L_n(\omega)$ are calculated by a Simpson and a
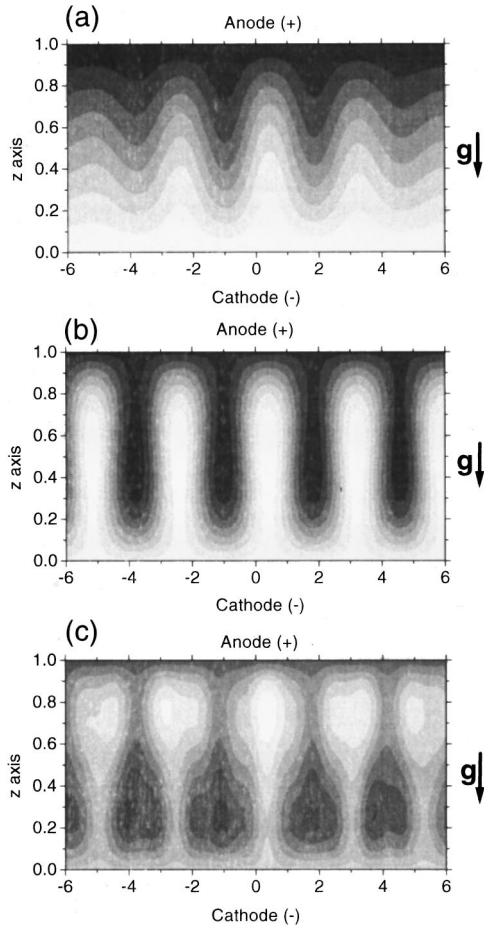
FIG. 11. Concentration profiles for the nonlinear case for various parameter values: (a) $R_{el} = 700$, $P_{el} = 10$; (b) $R_{el} = 1000$, $P_{el} = 10$; and (c) $R_{el} = 3000$, $P_{el} = 10$.

half Simpson formula depending on the parity of the parameter m. Once the spectral functions are determined, the original functions are calculated by the following equation:

$$\psi(x,z) = \sum_{n=1}^{\infty} \left(-4 \int_0^{\infty} [\text{Im}\tilde{\psi}_n(\omega)\cos\omega x + \text{Re}\tilde{\psi}_n(\omega)\sin\omega x] d\omega \right) \sin n\pi z, \quad (15)$$

and an analogous equation for $c(x,z)$. Equation (15) can be derived easily by considering the reality of the functions $\psi(x,z)$ and $c(x,z)$ and the parity introduced by the free surface boundary conditions. We must point out that although the numerical scheme requires the introduction of a discrete wave number grid, the grid values are only computational parameters and not physical parameters. For fixed initial conditions and small grid increment, the results do not depend on the choice of the grid values [33].

In Fig. 11 the solution of the nonlinear problem is presented for values of R_{el} above the critical value in the free surface case, after all the transients have died and the spectral functions have converged to a fixed value. For R_{el} close to the critical value the concentration profile is very similar to the linear case. By increasing R_{el} the concentration profile becomes more complicated and finally for high R_{el} values

takes a ''mushroom'' form. By comparing Fig. 11(c) with the experimental results of Fig. 3(a) we observe a very close similarity between the calculated behavior and the physicochemical response, even for these arbitrarily chosen values for the parameters. It can be seen that the two dimensional model for high R_{el} values reproduces qualitatively the behavior observed experimentally.

B. Under magnetic field

There are three main effects of the magnetic field on the behavior of the system, namely, the enlargement of the rolls, the tilting to the direction normal to the current flow, and the traveling of the rolls in the direction of the Lorenz force. The total current flowing in the solution containing a binary electrolyte, during a potentiostatic experiment, is a vector function of diffusion and electromigration currents. The convective phenomena, even though they do not enter explicitly the expression of the total current, determine the concentration distribution in the solution. Hence, the spatiotemporal character of the concentration distribution in the solution leads us to expect that the Lorenz body force, $\mathbf{F} = \mathbf{i} \times \mathbf{B}$, will not be constant in space and time but a spatiotemporal function, even when the applied magnetic field is constant.

Let us consider the electrolytic solution as a conducting liquid. Due to the low conductivity of the solution, no magnetic field is induced by the current. Also we can ignore the existence of displacement currents and assume electroneutrality. The total current flowing in the solution will be equal to the summation of the currents carried by cations and anions, that is,

$$\mathbf{i} = z_1 F \mathbf{j}_1 - z_2 F \mathbf{j}_2, \quad (16)$$

or, by using Eqs. (1) and (3),

$$\mathbf{i} = -(D_1 - D_2) F z_1 z_2 \nabla c. \quad (17)$$

In Eq. (17) we ignored the potential term under the condition that we are dealing with flows in the limiting (saturated) current region. Additionally, no convective term enters Eq. (17) due to electroneutrality. We must point out that under potentiostatic conditions the current flowing in the cell has both an x and a z component. Thus, due to the presence of the magnetic field, an additional forcing term (the Lorenz body force) will enter both Navier-Stokes equations, Eq. (8b). The equations of the original (unperturbed) variables under the effect of a magnetic field normal to the plane defined by the two electrodes will be

$$\frac{\partial u_x}{\partial t} + u_x \frac{\partial u_x}{\partial x} + u_z \frac{\partial u_x}{\partial z} = -\frac{1}{\rho_0} \frac{\partial p}{\partial x} + v \left(\frac{\partial^2 u_x}{\partial x^2} + \frac{\partial^2 u_x}{\partial z^2} \right) - \frac{i_z B}{\rho_0}, \quad (18a)$$

$$\frac{\partial u_z}{\partial t} + u_x \frac{\partial u_z}{\partial x} + u_z \frac{\partial u_z}{\partial z}$$

$$= -\frac{1}{\rho_0} \frac{\partial p}{\partial z} + v \left(\frac{\partial^2 u_z}{\partial x^2} + \frac{\partial^2 u_z}{\partial z^2} \right) - \frac{\rho}{\rho_0} g + \frac{i_x B}{\rho_0}. \quad (18b)$$

By using the analytic expression of the current, Eq. (17), and turning to the perturbation functions, the stream function equation becomes

$$\frac{\partial}{\partial t} \nabla^2 \psi + \frac{\partial(\psi, \nabla^2 \psi)}{\partial(x,z)} = \nabla^4 \psi - \frac{R_{el}}{P_{el}} \frac{\partial c}{\partial x} - F_{mag}\left(\frac{\partial^2 c}{\partial x^2} + \frac{\partial^2 c}{\partial z^2}\right),$$

(19)

where

$$F_{mag} = \frac{(D_1 - D_2)Fz_1z_2B\beta\delta^3}{\rho_0 v^2}$$

(20)

is the dimensionless forcing amplitude due to the magnetic field. By observing Eqs. (18) we can notice that there are two components of external forcing due to the magnetic field, one acting on the x direction and one on the z direction. The magnetic field is constant, but the current is a function of the concentration gradients in both directions.

By following the procedures of Sec. IV A we obtain the following equation for the spectral function of the stream function:

$$\kappa_n(\omega)\frac{d\widetilde{\psi}_n(\omega)}{dt} = -\kappa_n^2(\omega)\widetilde{\psi}_n(\omega) + i\omega\frac{R_{el}}{P_{el}}\widetilde{c}_n(\omega) + K_n(\omega)$$
$$+ \kappa_n(\omega)F_{mag}\widetilde{c}_n(\omega),$$

(21)

while Eq. (13b) remains the same.

By integrating Eqs. (21) and (13b), for low F_{mag} values, the concentration profile is similar to the case of the absence of the magnetic field. When F_{mag} becomes larger, the rolls are tilted from their original position and a modulation of the flow is also observed, leading to the enlargement of the rolls. Additionally, the rolls start to travel with constant speed toward the edge of the electrodes. The behavior of the system in the presence of the magnetic field is illustrated in Fig. 12. The three main effects of the magnetic field, namely, the tilting, the modulation, and the traveling of the rolls are reproduced by the model. By increasing the forcing amplitude, the traveling velocity of the rolls increases also. The increase of the traveling velocity as a function of F_{mag} is presented in Fig. 13. It can be seen that the velocity increases linearly with F_{mag}. By comparing Figs. 12 and 13 with the experimental results presented in Figs. 4 and 5 we can notice that most of the flow features are reproduced by the model equations.

V. DISCUSSION

Even though the model equations are a drastic simplification of the real system and the parameters for the numerical investigation were chosen arbitrarily, some useful conclusions could be drawn from this investigation. It is worth noting that our simplified system Eqs. (2) and (5) is similar to the equations describing the Bénard phenomenon [11,31]. This can be seen if we consider the following relationships:

$$c \to T, \quad D \to \kappa, \quad |dc/dz| \to |dT/dz|,$$

where T is the temperature and κ the thermal conductivity coefficient in the Bénard case. In the case of thermal convection, the behavior of the system is usually controlled by the variation of the Rayleigh number. This is accomplished by continuously varying the temperature difference between the upper and the lower fluid surface. In the electrochemical
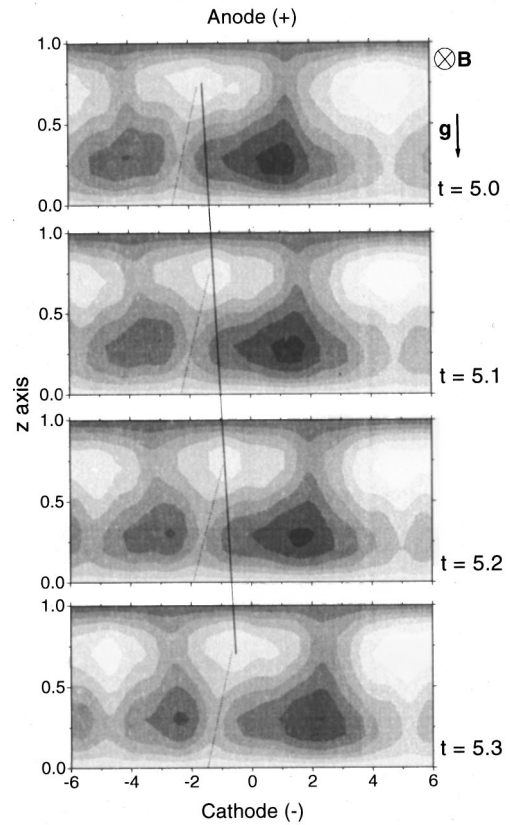

FIG. 12. Concentration profile under gravity and magnetic field. The rolls are enlarged, tilted, and travel towards the edge of the electrodes. $R_{el} = 1000$, $P_{el} = 10$, $F_{mag} = 100$.

case, a similar procedure would require the continuous variation of the concentration difference between the upper and the lower electrode. Unfortunately, this is not possible; when the system is in the limiting current region the concentrations have the fixed values of Eqs. (7). One might argue that the concentration difference could be altered continuously by varying the applied potential between the two electrodes. In this case, though, the effect of the potential should be included both in the boundary conditions, Eqs. (7), and the current expression, Eq. (22), and the problem would become extremely complex and difficult to deal with. The problem of continuously varying R_{el} by varying the concentration difference does not permit, at least at this stage, a direct compari-
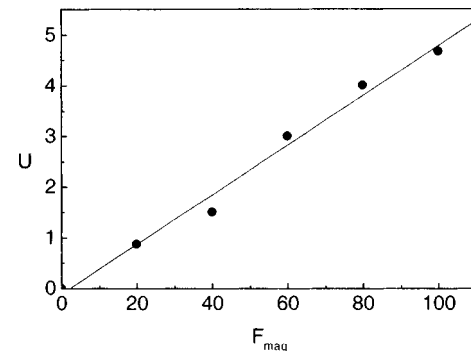

FIG. 13. Relationship between the traveling velocity of the rolls and the amplitude of the external forcing due to the magnetic field, F_{mag}. $R_{el} = 1000$, $P_{el} = 10$.

son of the critical values of this parameter between the modeling results and the experimental findings. This is the reason we give only a qualitative significance to the theoretical results. Nevertheless R_{el} can be affected by increasing the viscosity of the system with the addition of an electrochemically inert substance. Another parameter that could be varied is the distance between the electrodes. These effects are under study in our laboratory.

It is interesting to note also that natural convection is expected to take place in an electrochemical cell with only one reacting electrode. Levich [29] described to some extent the phenomenon in the case of a planar electrode, placed in parallel with the gravity force vector. The electrode was assumed to be a cathode. The length of the layer of variable concentration (diffusion layer) was found to be 0.03 cm. In our experimental setting, the distance of the electrodes is 0.03 cm. Thus, we can speculate that all our observations are performed in the area where the two diffusion layers of the electrodes are overlapped.

An analysis of the cell pattern formation in an electrochemical system was also presented in the past [34]. In that work, the authors present a model for the patterns formed on the electrode surface during electrodissolution under galvanostatic conditions. They consider the instability of the flow by supposing the coexistence of two superimposed fluids of different densities. The bottom fluid was adjacent to the electrode surface, where salt precipitation occurs, and the upper fluid was the electrolytic solution. In this sense, that system presents a Rayleigh-Taylor type of instability. The main difference with the system investigated in the present work is that we are dealing with formations in the electrolytic solution and not on the electrode surface. Additionally, the reason for variable density in our system is the concentration gradient between the two electrodes and not the superposition of fluid layers of different density. These two differences lead to a totally different formulation of the model equations.

Tilting, modulation, and traveling of the rolls during convection have been observed in a variety of systems. Among the most investigated ones is a driven fluid flow by an external spatially periodic forcing. In this system, constant current flows through an electrolytic solution, which is subjected to a time constant, spatially periodic magnetic force created by a linear arrangement of magnets under the bottom layer of the fluid. As the forcing increases the roll patterns in the fluid tend to tilt due to the development of shear flow [13–16,18–21. Similar behavior was observed in a system where the magnetic field was constant and the current flowing in the solution was spatially periodic [17]. Tilting and traveling of the rolls during convection was also observed in truncations of the full system describing the Rayleigh-Bénard convection, by varying the bifurcation parameters of the resulting system of ordinary differential equations [26]. A response that resembled this was observed also during resonance, leading to the break of parity of the solutions and bifurcation studies [35–37] and during investigations of magnetoconvection [23,24].

In the present study, we have shown that the electrochemical system under a concentration gradient between the electrodes can give rise to convective flow and roll pattern formation in the electrolytic solution. When this flow is subjected to an external forcing, due to the magnetic field, large scale flow develops, leading to the breaking of symmetry of the solutions. The external force is not constant in space and time, not due to the experimental settings but due to the physicochemical characteristics of the system. It can be seen from Eq. (19) that even though the magnetic field is kept constant during an experimental measurement, the forcing is not constant but a function of the concentration of the ionic species. By inspecting Eqs. (18) it can be noticed that the magnetic field does not act as an increase of the vertical concentration gradient but has an effect in both x and z direction. This fact leads to an additional coupling term between the Navier-stokes equations and the mass balance equation. When this coupling is large enough, the symmetry of the roll solutions breaks and the patterns tend to tilt and travel along the electrodes.

A detailed study remains to be done, in order to reveal the exact bifurcation characteristics of the system. Further experimental investigation of the physicochemical system and numerical exploration of the model equations for increasing values of R_{el} and F_{mag} will elucidate even more the mechanisms giving rise to pattern formation and bifurcations in electrochemical dynamical systems.

ACKNOWLEDGMENTS

[1] S. K. Scott, *Chemical Chaos* (Clarendon Press, Oxford, 1991), p. 195.

[2] T. Fink, R. Imbihl, and G. Ertl, J. Chem. Phys. **91**, 5002 (1989).

[3] H. H. Rotermund, S. Jakubith, A. von Oertzen, and G. Ertl, J. Chem. Phys. **91**, 4942 (1989).

[4] D. R. Chialvo, R. F. Gilmour, and J. Jalife, Nature (London) **343**, 635 (1990).

[5] T. Kohoner, *Self-Organization and Associative Memory* (Springer, New York, 1984), p. 123.

[6] S. Amari and T. S. Han, IEEE Trans. Inf. Theory **35**, 217 (1989).

[7] S. Nakabayashi and A. Kira, J. Phys. Chem. **96**, 1021 (1992).

[8] S. Nakabayashi, N. Sugiyama, I. Yagi, and K. Uosaki, Chem. Phys. **205**, 269 (1996).

[9] S. Nakabayashi, K. Zama, and K. Uosaki, J. Electrochem. Soc. **143**, 2258 (1996).

[10] C. Normand and Y. Pomeau, Rev. Mod. Phys. **49**, 581 (1977).

[11] S. Chandrasekhar, *Hydrodynamic and Hydromagnetic Stability* (Dover, New York, 1981), pp. 16 and 429.

[12] M. Treitereid, Phys. Rev. E **50**, 1219 (1994).

[13] P. N. Guzdar, J. M. Finn, A. V. Rogalsky, and J. F. Drake, Phys. Rev. E **49**, 2062 (1994).

[14] R. Braun, F. Feudel, and P. Guzdar, Phys. Rev. E **58**, 1927 (1998).

[15] J. F. Drake, J. M. Finn, P. Guzdar, V. Shapiro, and V. Shenvchenko, Phys. Fluids B **4**, 488 (1992).

[16] J. M. Finn, J. F. Drake, and P. N. Guzdar, Phys. Fluids B **4**, 2758 (1992).

[17] J. Sommeria, J. Fluid Mech. **170**, 139 (1986).

[18] P. Tabeling, O. Cardoso, and B. Perin, J. Fluid Mech. **213**, 511 (1990).

[19] A. Thess, Phys. Fluids A **4**, 1385 (1992).

[20] F. V. Dolzhanskii, V. A. Krymov, and D. Yu. Manin, J. Fluid Mech. **241**, 705 (1992).

[21] F. Feudel and N. Seehafer, Phys. Rev. E **52**, 3506 (1995).

[22] M. Sano, K. Sato, S. Nasuno, and H. Kokubo, Phys. Rev. A **46**, 3540 (1992).

[23] P. C. Matthews, M. R. E. Proctor, A. M. Rucklidge, and N. O. Weiss, Phys. Lett. A **183**, 69 (1993).

[24] M. R. E. Proctor, N. O. Weiss, D. P. Brownjohn, and N. E. Hurlburt, J. Fluid Mech. **280**, 227 (1994).

[25] R. Schmitz and W. Zimmermann, Phys. Rev. E **58**, 3145 (1998).

[26] L. N. Howard and R. Krishnamurti, J. Fluid Mech. **170**, 385 (1986).

[27] R. H. Muller, in *Advances in Electrochemistry and Electrochemical Engineering*, edited by P. Delahey and C. Tobias (Wiley, New York, 1973), Vol. 9, p. 281.

[28] M. Born and E. Wolf, *Principles of Optics* (Pergamon, Oxford, 1975), p. 321.

[29] V. G. Levich, *Physicochemical Hydrodynamics* (Prentice-Hall, Englewood Cliffs, NJ, 1962), pp. 53 and 127.

[30] S. Nakabayashi, M. Yanagida, and H. Uosaki, J. Phys. Chem. **100**, 714 (1996).

[31] F. H. Busse, in *Hydrodynamic Instabilities and the Transition to Turbulence*, edited by H. L. Swinney and J. P. Gollup, Topics in Applied Physics Vol. 45 (Springer-Verlag, Berlin, 1981), p. 97.

[32] R. B. Bird, W. E. Steward, and E. N. Lightfoot, *Transport Phenomena* (Wiley, New York, 1960), p. 74.

[33] A. V. Getling, J. Fluid Mech. **130**, 165 (1983).

[34] M. A. Tenan, O. Teschke, M. U. Kleinke, and F. Galembeck, Langmuir **6**, 1640 (1990).

[35] J. Prat, J. M. Massaguer, and I. Mercader, Phys. Fluids **7**, 121 (1995).

[36] J. Prat, I. Mercader, and E. Knobloch, Phys. Rev. E **58**, 3145 (1998).

[37] E. Zienicke, N. Seehafer, and F. Feudel, Phys. Rev. E **57**, 428 (1998).